Journal of Hazardous Materials 186 (2011) 645–650

Contents lists available at ScienceDirect

Journal of Hazardous Materials

journal homepage: www.elsevier.com/locate/jhazmat

# Use of electrochemical techniques to characterize methamidophos and humic acid specifically adsorbed onto Pt and PtO films

Andréia P. Silva, Adriana E. Carvalho, Gilberto Maia*

*Department of Chemistry, Universidade Federal de Mato Grosso do Sul, Caixa Postal 549, Campo Grande, MS 79070-900, Brazil*

ARTICLE INFO

*Article history:*
Received 30 September 2010
Received in revised form
11 November 2010
Accepted 12 November 2010
Available online 20 November 2010

*Keywords:*
Cyclic voltammetry
Electrochemical impedance spectroscopy
Methamidophos
Humic acid
Specific adsorption

ABSTRACT

Cyclic voltammetry (CV) and electrochemical impedance spectroscopy (EIS) were employed to study methamidophos (MAP) and humic acid (HM) specifically adsorbed onto Pt and PtO films in pH-7.0 universal buffer. The approach was found to be sufficiently selective for use in studies involving adsorption of species in environmental systems (e.g., soil minerals), typically evaluated by batch experiments and high performance liquid chromatography (HPLC) or gas chromatography (GC). The proposed method allowed quantification of active hydrogen adsorption sites blocked by HM, both when this compound is adsorbed alone or co-adsorbed with MAP. At higher amounts of MAP in the adsorption solution, the compound was co-adsorbed more effectively than HM (kept at constant concentration). In the case of sequential specific adsorption, the first compound adsorbed typically predominates over the second. EIS was more effective for determining the number of blocked active sites on Pt than CV, which was superior for PtO films.



## 1. Introduction

Sorption onto immobile mineral surfaces is often the key process controlling mobility and degradation in subsurface environments [1]. A number of factors contribute to the partitioning of pesticides between solutions and solid phases. These factors include general conditions of solutions (e.g., pH, concentration of pesticides), soil mineral content, natural organic matter (NOM) content, and characteristics of the mineral surfaces [2]. NOM may enhance or retard the migration of pesticides in subsurface environmental systems, depending on system composition (e.g., quantity and characteristics of organic ligands) [1]. The main components of NOM are humic substances (HS). Dissolved humic substances (DHS) are composed of a mixture of humic and fulvic acids (HM and FV) of different molecular weights [3].

Pollution of wastewater by organophosphorous pesticides is a common problem around the world and a focus of considerable research effort. Organophosphorous compounds (OPCs), extensively used as insecticides, are known to inhibit acetylcholinesterase. Most are highly toxic to humans and other mammals. Due to their high chemical stability and toxicity, OPCs resist natural decomposition and biodegradation [4,5]. Moreover, owing to their high polarity and dissolution capacity, they can easily infiltrate the soil and migrate to other locations [4]. Methamidophos (O,S-dimethyl phosphoramidothioate, MAP) is an OPC with a broad spectrum of activity as an insecticide–acaricide through inhibition of acetyl-cholinesterase activity in insects and mammals, and is widely used on vegetables, corn, and some other crops [6].

The involvement of mineral surfaces in MAP sorption and adsorption has been well established by numerous studies, including those on MAP movement and sorption in sandy loam and clay loam soils [1], MAP sorption by alluvial soils containing components such as clays or Al/Fe oxides [2], MAP adsorption, desorption, and mobility in sandy loam and clay soils [7], while OPC adsorption phenomena have been investigated by equilibrating aqueous pesticide (including MAP) solutions with six certified soils of varied physico-chemical characteristics [8].

The studies of MAP sorption and desorption by soils have largely been based on batch experiments with bulk samples and on quantification of MAP using GC [1,2,9] or HPLC [10].

MAP interaction with different mineral surfaces has been previously reported, as has the influence of NOM on MAP sorption, adsorption, and desorption. Recently, we conducted studies involving adsorption of propiconazole (PPC) and HM onto Pt and PtO films [11], as well as adsorption of arsenic and HM onto these types of film [12], using cyclic voltammetry (CV) and cyclic massograms. To the best of our knowledge, no previous studies have investigated MAP specifically adsorbed onto Pt and PtO films or the influence of HM, a component of NOM, on MAP co-adsorbed onto these surfaces using CV and electrochemical impedance spectroscopy (EIS) in pH-7.0 universal buffer solution. The rationale behind conducting this

* Corresponding author. Tel.: +55 67 33453551; fax: +55 67 33453552.
*E-mail address:* gmaia@nin.ufms.br (G. Maia).

0304-3894/$ – see front matter © 2010 Elsevier B.V. All rights reserved.
doi:10.1016/j.jhazmat.2010.11.059

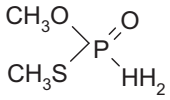

**Scheme 1.** Chemical structure of MAP.

type of study is to develop an alternative model for experiments aimed at detecting specifically adsorbed pesticides in soil samples, so as to further clarify the factors influencing pesticide adsorption/desorption.

## 2. Experimental

Electrochemical and EIS studies were carried out using a three-electrode glass cell with a working electrode consisting of a Pt disc (0.1642 $cm^2$ in geometric area) embedded in Teflon (polycrystalline Pt). A reversible hydrogen electrode (RHE) was employed as the reference electrode and the counter-electrode consisted of a Pt plate (Degussa). Electrochemical and EIS measurements were determined using an Autolab potentiostat/galvanostat (model PGSTAT128N) equipped with a FRA2.X module. The EIS experiments were conducted at fixed potentials (0.25, 0.55, 0.9, and 1.15 V vs. RHE) with a potential perturbation of 10 mV (rms), within the frequency range of 40 mHz to 10 kHz. NOVA 1.5 Autolab (2009) software was used to simulate the behavior of equivalent circuits of the interface in the presence of specific adsorption, and the parameters of these circuits were fitted to the measured spectra using a non-linear least squares program.

The working electrode was electrochemically cleaned in ultrapure $N_2$-saturated pH-7.0 universal buffer (or 0.5 M $H_2SO_4$) solution, as described in our previous study [11]. The ratio-of-roughness factor [11], determined by the amount of hydrogen desorbed into pH-7.0 universal buffer, was $1.64 \pm 0.03$, calculated based on the relation 2.10 C $m^{-2}$ for the formation of a H monolayer on a Pt surface [13].

MAP (Scheme 1) was obtained from Riedel-de-Haën (analytical standard), HM from Aldrich (technical grade), and $H_2SO_4$ from Merck (p.a.). The universal buffer [14] (pH 7) contained boric acid, citric acid, trisodium phosphate, and $Na_2SO_4$ (to maintain an ionic force of 0.5 M) (all chemicals from Merck). The solutions were prepared using Milli-Q water and purged for 20 min with ultrapure nitrogen (White Martins) prior to each experiment. The specific adsorption procedure entailed immersing a cleaned Pt or PtO film electrode for 20 min in seven freshly prepared aqueous solutions (see Table 1, which also lists the electrodes and specifically adsorbed species). The open-circuit potential ($E_{oc}$) of the aqueous solutions in contact with the Pt or PtO films was found to be approximately 0.90 V. After immersion, the electrode was copiously washed with water and transferred to an electrochemical cell containing pH-7.0 universal buffer. The other experimental conditions were as described in our previously published study [11].

We made the assumption that the PtO films formed were similar to those produced in our previously published experiments [11,12], with the only difference in the present study being the use of pH-7.0 universal buffer solution.

**Table 1**
Nomenclature and composition of solutions used during specific adsorption, and electrode designation of modified electrodes with specifically adsorbed species.

| Solution[a] | Composition | Electrode designation |
|---|---|---|
| S1 | 10 mg carbon $L^{-1}$ HM | Pt/HM or PtO/HM |
| S2 | $1 \times 10^{-6}$ M MAP | Pt/MAP or PtO/MAP |
| S1/S2[b] | 10 mg carbon $L^{-1}$ HM/$1 \times 10^{-6}$ M MAP | Pt/HM/MAP or PtO/HM/MAP |
| S2/S1[b] | $1 \times 10^{-6}$ M MAP/10 mg carbon $L^{-1}$ HM | Pt/MAP/HM or PtO/MAP/HM |
| S3 | $1 \times 10^{-6}$ M MAP and 10 mg carbon $L^{-1}$ HM | Pt/M1 or PtO/M1 |
| S4 | $5 \times 10^{-6}$ M MAP and 10 mg carbon $L^{-1}$ HM | Pt/M2 or PtO/M2 |
| S5 | $1 \times 10^{-5}$ M MAP and 10 mg carbon $L^{-1}$ HM | Pt/M3 or PtO/M3 |
| S6 | $5 \times 10^{-5}$ M MAP and 10 mg carbon $L^{-1}$ HM | Pt/M4 or PtO/M4 |
| S7 | $1 \times 10^{-4}$ M MAP and 10 mg carbon $L^{-1}$ HM | Pt/M5 or PtO/M5 |

[a] pH values approximately 5.0 for all solutions.
[b] In cases of sequential adsorption, the electrode was copiously washed with water between adsorptions.

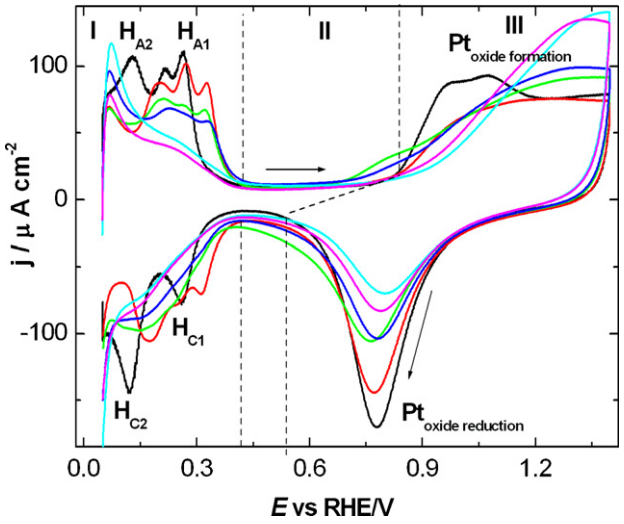


**Fig. 1.** First CVs for (a, in 0.5 M $H_2SO_4$) pristine Pt (—) and (b–f, in pH-7.0 universal buffer solution) (b) pristine Pt (▬), (c) Pt/HM (▬), (d) Pt/MAP (▬), (e) Pt/M4 (▬), and (f) Pt/M5 (▬). The modified electrode surfaces were washed with water (5 times) before CV acquisition. Scans start at 0.05 V vs. RHE in the positive potential direction. Scan rate: 100 mV $s^{-1}$.

## 3. Results and discussion

### 3.1. CV study of HM and MAP specifically adsorbed onto Pt

Fig. 1 shows the behavior of the first CV cycle in 0.5 M $H_2SO_4$ for pristine Pt, as well as in pH-7.0 universal buffer for pristine Pt and four Pt electrodes modified by specific adsorption from four different aqueous solutions (see Section 2). The CV regions delimited in Fig. 1 have been described elsewhere [11,12]. Briefly, region I is related to UPD hydrogen adsorption/desorption; region II, to the double layer charging/discharging of the Pt surface; region III, to the oxidation of the Pt surface to form a Pt oxide, and possibly also related to the oxidation of the adsorbed compounds and subsequent reduction of Pt oxide in the negative potential scan direction.

For both pair of peaks ($H_{A2}$, $H_{A1}$ and $H_{C2}$, $H_{C1}$) [11,12], displacement was observed toward more positive potential for pristine Pt in the presence of pH-7.0 universal buffer, in comparison to 0.5 M $H_2SO_4$ (curves b–a, Fig. 1). An overall decrease in the current densities involving UPD hydrogen desorption/adsorption was also revealed by comparing the four modified Pt electrodes with pristine Pt (Fig. 1). This suggests interactions between Pt surface sites and both HM and MAP—interactions that modify both the oxidation of adsorbed hydrogen ($H_{A2}$, $H_{A1}$) and the reduction related to hydrogen adsorption ($H_{C2}$, $H_{C1}$).

The increase in current densities observed in region II relative to pristine Pt (Fig. 1) suggests that compounds adsorbed onto the Pt surface are oxidized (positive potential scan direction) and reduced (negative potential scan direction) in this region, and that these oxidation/reduction current densities are mainly affected for the Pt/HM and Pt/MAP electrodes (Fig. 1).

In region III (positive potential scan direction), changes in the current densities are also seen, with a decrease in current densities in the potential range of 0.88–1.13 V relative to pristine Pt in 0.5 M $H_2SO_4$ (Fig. 1). At potentials higher than 1.13 and 1.07 V, the current densities become significantly higher relative to pristine Pt in 0.5 M $H_2SO_4$ (curve a, Fig. 1) and pH-7.0 universal buffer (curve b, Fig. 1), respectively. The former dependence suggests that the adsorbed compounds block the active sites for Pt oxidation in this region and that this blockage depends on the nature of the compound, whereas the latter dependence suggests that the adsorbed compounds might be oxidized in this potential range. Upon reversing the potential scan toward the negative direction, differences in region III were detected, primarily due to a decrease in the current densities for the reduction peak at 0.70 V (Fig. 1). (Patterns followed by current densities for different adsorbed compounds are described in section SI).

We have recently proposed a mechanism describing the adsorption and oxidation of HM on Pt [11] and it should be stressed that the oxidation products of HM can be again adsorbed onto the Pt surface [12]. It is possible that in pH-7.0 universal buffer solutions the first electron transfer to adsorbed HM may occur in the potential region of 0.8 V and the second electron transfer at 1.3 V, whereas some reduction of oxidized HM products may take place in the potential region of 0.55 V.

MAP has been reported to have a greater tendency to protonate at higher p$K_a$ values (p$K_a$ 10) [2,9,15] because of its weak basic molecule. MAP can be ionized by protonation of either the P=O or the $-NH_2$ group (reactive functional groups) at pH 4–8 [2,9,15]. Protonation may promote adsorption of MAP by soil organic matter or siliceous clay through coordinate bonds [9]. However, protonated species of MAP may undergo a series of rearrangements because of charge distribution and charge delocalization among P, N, and O atoms [9,15]. Under the effects of this charge delocalization, MAP does not acquire a true protonated $NH_3^+$ group, and there is a net positive charge only at the N atom that constituted the cationic domain in MAP [9,15]. The polarity of protonated MAP molecules is therefore weak, and MAP adsorption is thought not to occur through cation exchange reaction (substituting the metal ions fixed on the surfaces of soil colloids), but possibly by the action of forces between molecules, such as van der Waals forces and hydrogen bonds [16].

We are assuming that at pH 5.0 (the pH value of our specific adsorption solutions) the protonated MAP species **1** or **2**, adsorbed onto the Pt (or PtO film) surface by the –OH (or $-O^-$) moiety or $-NH_2$, will be oxidized as follows:

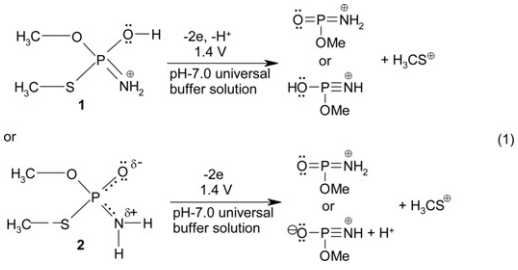


(1)

Sing et al. [15] and Martínez-Huitle et al. [17] suggested that $-SCH_3$ is a leaving group, but we are not assuming that both electrons are necessarily removed in a single step.

### 3.2. EIS study of HM and MAP specifically adsorbed onto Pt

Fig. 2 illustrates the behavior of the capacitance spectra (40 mHz to 10 kHz, with frequencies decreasing clockwise) measured at 0.25 and 1.15 V and at 0.55 and 0.9 V (Fig. S3) in 0.5 M $H_2SO_4$ for pristine Pt, and in pH-7.0 universal buffer for pristine Pt and nine Pt

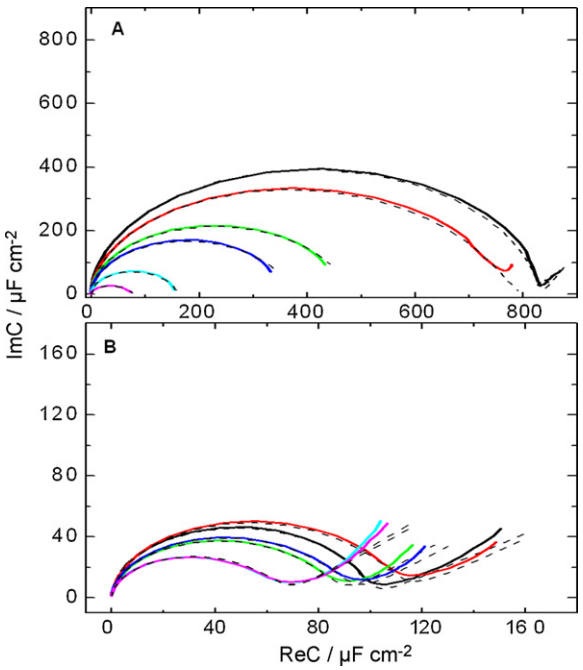


**Fig. 2.** Capacitance spectra (10 kHz to 40 mHz, clockwise) for (a, in 0.5 M $H_2SO_4$) pristine Pt (—) and (b–f, in pH-7.0 universal buffer solution) (b) pristine Pt ( ), (c) Pt/HM ( ), (d) Pt/MAP ( ), (e) Pt/M4 ( ), and (f) Pt/M5 ( ). The modified electrode surfaces were washed with water (5 times) before EIS acquisition. Constant potentials for EIS acquisition at (A) and (B): 0.25 and 1.15 V vs. RHE, respectively. Dashed lines represent spectra calculated (adjusted) by a non-linear least squares program for the circuits described in Section 3.2.

electrodes modified by specific adsorption from seven different aqueous solutions (see Section 2). These four values of constant potential for the EIS study were selected so as to cover three representative points of the voltammetric studies discussed in Section 3.1 (0.25, 0.55, and 1.15 V) and the region of $E_{oc}$ (0.9 V) for the electrodes studied.

The measured spectra represented graphically in this study are based on calculations and plots of the complex function $C(\omega) = Y(\omega)/(i\omega) = 1/([Z(\omega) - Z(\omega \to \infty)]Ai\omega)$, where $\omega$, $Z(\omega \to \infty) = R_s$, $A$, and $i$ represent angular frequency, solution resistance, electrode area, and imaginary unit, respectively. Because of its physical meaning, $C(\omega)$ is termed 'interfacial capacitance' and, being a complex quantity, can be plotted only in complex representation [18,19].

As suggested by Kerner, Pajkossy, and Kolb [19–20], the measured impedance spectra for circuits $[R_s(C_{dl}[R_{ad}W_{ad}C_{ad}])]$, $[R_s(Q_{dl}[R_{ad}W_{ad}C_{ad}])]$, or $[R_s(Q_{dl}[R_{ad}C_{ad}])]$ can be simulated in the potential regions of specific adsorption, where $C_{dl}$, $R_{ad}$, $W_{ad}$, $C_{ad}$, and $Q_{dl}$ represent double-layer capacitance, adsorption resistance, Warburg impedance (diffusional impedance associated with species adsorption), adsorption capacitance, and phase constant element involving an $n$ exponent to represent $C_{dl}$, respectively. The adsorption-related elements of this circuit can be interpreted by the classical adsorption impedance theories devised by Ershler, Frumkin and Melik-Gaykasyan, and Lorenz and Möckel (see references cited in [18–20]), which yield the expected capacitance spectrum $C(\omega)$:

$$C(\omega) = \frac{1}{i\omega(Z(\omega) - R_s)} = C_{dl} + \frac{C_{ad}}{1 + \sigma_{ad}C_{ad}(i\omega)^{1/2} + R_{ad}C_{ad}i\omega} \quad (1)$$

where $\sigma_{ad}$ is the coefficient of the Warburg impedance defined by $Z(W_{ad}) = \sigma_{ad}(i\omega)^{-1/2}$ [18,19].

The $C(\omega)$ spectra are plotted in the complex plane as circular (Figs. 2 and S3) or distorted arcs [18]; semicircular and 'depressed'

arcs at the extremes of slow and fast (diffusion-controlled) adsorption, respectively; or skewed arcs in intermediate, mixed kinetics cases (cf. Fig. 1 in [18,19]). Irrespective of adsorption kinetics, the second term of Eq. (1) approaches zero at high frequencies, revealing that the high frequency limit is equal to the double-layer capacity ($C(\omega \to \infty) = C_{HF} = C_{dl}$), whereas at low frequencies the sum of double-layer capacity and adsorption capacity can be measured ($C(\omega \to 0) = C_{LF} = C_{dl} + C_{ad}$) [19]. These capacities have the physical meanings $C_{dl} = (\partial q^M/\partial E)_{\Gamma}$ and $C_{LF} = dq^M/dE$, respectively, where $q^M$ and $\Gamma$ represent excess charge of the metal and surface excess of the adsorbate, respectively [18]. The denominator of the second term of Eq. (1) increases with decreasing adsorbate concentration (cf. Eq. (3) in [19]), and thus the $C(\omega)$ spectra shrink toward $C_{dl}$ at high frequencies as the concentration of adsorbate falls [21].

As seen in Figs. 2 and S3, $C(\omega)$ spectra are semicircles, suggesting an extreme of slow (diffusion-controlled) adsorption, revealing overall shrinkage of spectra toward $C_{dl}$ as the concentration of adsorbate decreases as a result of previous specific adsorption of compounds (a process that blocks electrode surface to hydrogen adsorption at 0.25 V), adsorption of anionic species present in pH-7 universal buffer at 0.55 V, and oxygen adsorption at 0.9 and 1.15 V. The ReC values intercepting the ordinate near zero for $\omega \to \infty$ can be attributed to the elevated concentration of adsorbate – 0.5 M $H_2SO_4$ or pH-7.0 universal buffer (ionic force, 0.5 M) – while also influencing spectra by shaping these as semicircles, thus suggesting an extreme of slow (diffusion-controlled) adsorption of adsorbate by virtue of this elevated concentration.

Tables S1–S4 show the values of equivalent circuit elements obtained with the non-linear least squares program. These tables provide a broader view of the theoretical (simulated) and experimental EIS results shown in Figs. 2 and S3.

The $R_s$ and $R_{ad}$ values (Tables S1–S4) are small (but non-null) and can generally be considered equal to 5 $\Omega\,cm^2$. Although $R_{ad}$ is typically non-null in systems having adsorbed ions (ref. 7 cited in [18]), in the systems studied in [18] $R_{ad}$ played no relevant role, as is the case in the present system. $C_{dl}$ or $Q_{dl}$ coupled with an $n$ exponent to represent $C_{dl}$ are generally around 20 $\mu F\,cm^{-2}$ [18], with some exceptions at lower values (Pt/HM electrode, Table S1, and Pt/M4 electrode, Table S2) and higher values (pristine Pt electrode in 0.5 M $H_2SO_4$, Table S4). The values of $n$ range from 0.34 (Pt/M2 electrode, Table S3) to 0.97 (electrode Pt/MAP, Table S2). $W_{ad}$ values vary according to the modified electrodes, and were decreased overall for Pt/M2-Pt/M5 (Table S1) and Pt/M1-Pt/M5 (Table S4) electrodes. This suggests a decrease in the spread of those species specifically adsorbed on these electrodes (hydrogen and oxygen species, respectively).

The largest differences were observed for $C_{ad}$, especially for EIS experiments conducted at 0.25 (Table S1) and 1.15 V (Table S4). For EIS experiments conducted at 0.25 V (Table S1), high $C_{ad}$ values were calculated for pristine Pt in the presence of 0.5 M $H_2SO_4$ and pH-7.0 universal buffer. For the electrode modified with HM (Pt/HM), $C_{ad}$ was much lower than that obtained for pristine Pt with pH-7.0 universal buffer. Moreover, $C_{ad}$ values were generally decreased for the Pt/M1-Pt/M5 electrodes—a similar pattern of decline was observed for $C_{ad}$ for the same electrodes in EIS experiments conducted at 0.55 (Table S2), 0.90 (Table S3), and 1.15 V (Table S4). This behavior is consistent with the decrease in the number of active sites for adsorption of species in pH-7.0 universal buffer (hydrogen, anions, oxygen species), owing to the presence of compounds previously specifically adsorbed in solutions S1–S7.

Based on the occurrence of major changes detected for $C_{ad}$ (and smaller variations detected for $W_{ad}$) in EIS experiments conducted at 0.25 and 1.15 V, we calculated the charge densities at these two point potentials using a simple expression that relates $C_{ad}$ to charge density:

$$q = C_{ad}E \tag{2}$$

The charge densities in two regions (I and III) of the cyclic voltammetric results shown in Figs. 1 and S2 were calculated as described in [11]. These charge densities were used to calculate the densities of active sites blocked by spontaneously adsorbed compounds in regions I and III, and at two point potentials (0.25 and 1.15 V), ${N_{AS,I}}^{bloc}$ and ${N_{AS,III}}^{bloc}$, respectively, using the equations [22]:

$${N_{AS,I}}^{bloc} = ({Q_H}^{blank}(\text{or } {q_{0.25\,V}}^{blank}) - {Q_H}^{des}(\text{or } {q_{0.25\,V}}^{mod\ elec})) \left(\frac{N_A}{F}\right) \tag{3}$$

$${N_{AS,III}}^{bloc} = ({Q_{Pt\ ox\ red}}^{blank}(\text{or } {q_{1.15\,V}}^{blank}) - Q_{Pt\ ox\ red}(\text{or } {q_{1.15\,V}}^{mod\ elec})) \left(\frac{N_A}{2F}\right) \tag{4}$$

where ${Q_H}^{blank} = 210\,\mu C\,cm^{-2}$ is the value obtained for pristine Pt in 0.5 M $H_2SO_4$ and pH-7 universal buffer (for the meaning of ${Q_H}^{blank}$ and $Q$, see [11]), ${q_{0.25\,V}}^{blank} = 200\,\mu C\,cm^{-2}$, ${q_{1.15\,V}}^{blank} = 130\,\mu C\,cm^{-2}$, ${q_{0.25\,V}}^{mod\ elec}$, and ${q_{1.15\,V}}^{mod\ elec}$ were obtained using Eq. (2) for modified electrodes, $N_A$ is the Avogadro number, and $F$ is the Faraday constant.

The ${N_{AS,I}}^{bloc}$ and ${N_{AS,III}}^{bloc}$ values shown in Table 2 vary with the specifically adsorbed compounds, rising overall for the Pt/M1-Pt/M5 electrodes. Where UPD hydrogen desorption occurs at lower positive potentials, it is generally twice as high for ${N_{AS,I}}^{bloc}$ calculated using data obtained from $q$ instead of $Q$. This may suggest that the higher sensitivity achieved by using results from EIS experiments, rather than from CV, in this potential region, can probably be explained by the additional current densities present in the potential region of 0.05–0.15 V in the case of CV. The number of active sites blocked by HM at the Pt/HM electrode was calculated as $468 \times 10^{12}$ sites $cm^{-2}$, and those blocked by MAP at the Pt/MAP electrode as $673 \times 10^{12}$ sites $cm^{-2}$. Assuming the occurrence of co-adsorption, we considered that the sites for hydrogen adsorption at the Pt/HM/MAP and Pt/MAP/HM electrodes are predominantly blocked by HM and MAP, respectively, as these are the earliest compounds to be adsorbed onto those electrodes—a feature that should yield values similar to those obtained for HM and MAP when these are individually adsorbed, with the difference in ${N_{AS,I}}^{bloc}$ ($24 \times 10^{12}$ and $84 \times 10^{12}$ sites $cm^{-2}$) being attributed to co-adsorption of MAP and HM, which block the sites for hydrogen adsorption. In the case of the Pt/M1 electrode, we assumed that $468 \times 10^{12}$ sites $cm^{-2}$ were blocked by specific adsorption of HM, whereas the remaining value (i.e., $(504–468) \times 10^{12}$ sites $cm^{-2} = 36 \times 10^{12}$ sites $cm^{-2}$) was attributed to co-adsorption of MAP due to the presence of MAP at low concentration in the S3 solution used for specific adsorption. For the Pt/M2-Pt/M5 electrodes, we assumed co-adsorption of HM (with MAP) to be less than $468 \times 10^{12}$ sites $cm^{-2}$, although it was not possible to quantify this figure. The highest number of active sites blocked by MAP was found for the Pt/MAP and Pt/M5 electrodes ($637 \times 10^{12}$ sites $cm^{-2} = (1105–468) \times 10^{12}$ sites $cm^{-2}$).

At high positive potentials where oxide formation occurs ($PtO_x$ formation in region III; see Table 2), similar values were generally observed for ${N_{AS,III}}^{bloc}$ calculated using data from $q$ instead of $Q$. Following the same reasoning outlined in the previous paragraph, the highest number of active sites blocked by HM was found for the Pt/HM electrode ($162 \times 10^{12}$ sites $cm^{-2}$) and the highest number of those blocked by MAP was found for the Pt/MAP and Pt/M5 electrodes ($150 \times 10^{12}$ sites $cm^{-2}$).

**Table 2**
Number of blocked active sites estimated from the cyclic voltammograms depicted in Figs. 1 and S2, and from $C_{ad}$ values obtained from spectra calculated from EIS results at 0.25 and 1.15 V in Figs. 2 and S3.

| Interface | $N_{AS,I}{}^{bloc}$ ($\times 10^{-12}$ sites cm$^{-2}$) | $N_{AS,I}{}^{bloc}$ ($\times 10^{-12}$ sites cm$^{-2}$)[a] | $N_{AS,III}{}^{bloc}$ ($\times 10^{-12}$ sites cm$^{-2}$) | $N_{AS,III}{}^{bloc}$ ($\times 10^{-12}$ sites cm$^{-2}$)[b] |
|---|---|---|---|---|
| Pristine Pt (0.5 M $H_2SO_4$) | 0 | 0 | 0 | 0 |
| Pristine Pt (pH-7 universal buffer solution) | 0 | 0 | 0 | 0 |
| Pt/HM | 200 | 468 | 194 | 162 |
| Pt/MAP | 212 | 673 | 175 | 127 |
| Pt/HM/MAP | 462 | 492 | 250 | 139 |
| Pt/MAP/HM | 331 | 757 | 116 | 159 |
| Pt/M1 | 131 | 504 | 187 | 195 |
| Pt/M2 | 474 | 897 | 184 | 282 |
| Pt/M3 | 462 | 833 | 219 | 213 |
| Pt/M4 | 418 | 993 | 362 | 312 |
| Pt/M5 | 630 | 1105 | 294 | 314 |

[a] Determined from $C_{ad}$ values obtained from spectra calculated from EIS results at 0.25 V.
[b] Determined from $C_{ad}$ values obtained from spectra calculated from EIS results at 1.15 V.

### 3.3. CV and EIS study of HM and MAP specifically adsorbed onto PtO films

Fig. 3 shows the behavior of the first CV cycle in 0.5 M $H_2SO_4$ for a pristine PtO film, as well as in pH-7.0 universal buffer for a pristine PtO film and four PtO film electrodes modified by specific adsorption from four different aqueous solutions (see Section 2). Initially, significantly lower current densities were detected relative to Pt, owing to the presence of a PtO film (compare Figs. 1 and 3). In the scan toward positive potentials, the current densities were lower in the potential region of 0.82–1.40 V. A decrease in current densities was detected for the Pt/HM, Pt/MAP, and PtO/M4-PtO/M5 electrodes. These responses confirm co-adsorption of HM and MAP, and greater amounts of MAP are possibly adsorbed at increasing concentrations of the solutions used for specific adsorption (Fig. 3). In the scan toward negative potentials, the current densities are decreased (in modulus) in the potential region of 1.32–0.75 V. These comparisons are made in relation to pristine PtO film.

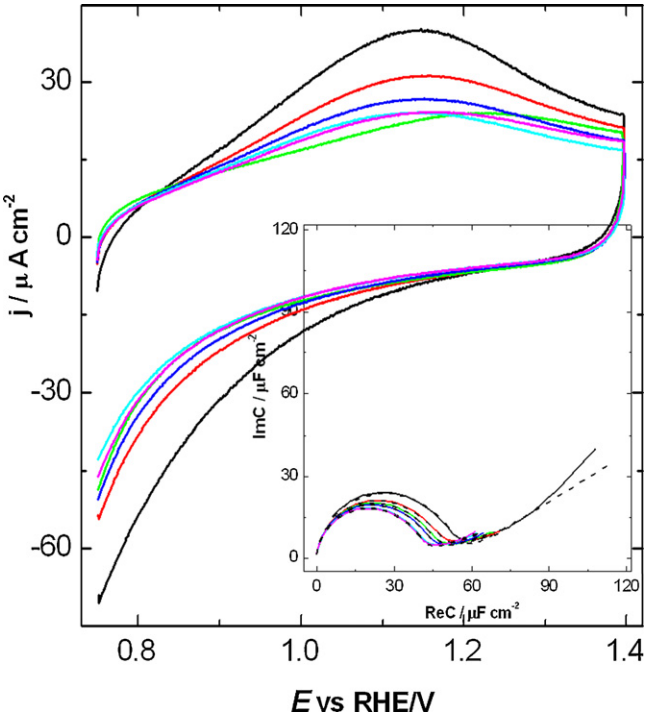


**Fig. 3.** First CVs for (a, in 0.5 M $H_2SO_4$) pristine PtO film (—) and (b–f, in pH-7.0 universal buffer solution) pristine PtO film (—), (c) PtO/HM (—), (d) PtO/MAP (—), (e) PtO/M4 (—), and (f) PtO/M5 (—). The modified electrode surfaces were washed with water (5 times) before CV acquisition. Scans start at 0.75 V vs. RHE in the positive potential direction. Scan rate: 100 mV s$^{-1}$. Inset: capacitance spectra (10 kHz to 40 mHz, clockwise) for (a, in 0.5 M $H_2SO_4$) pristine PtO film (—) and (b–f, in pH-7.0 universal buffer solution) pristine PtO film (—), (c) Pt/HM (—), (d) Pt/MAP (—), (e) Pt/M2 (—), and (f) Pt/M5 (—). The modified electrode surfaces were washed with water (5 times) before EIS acquisition. Constant potential for EIS acquisition: 1.15 V vs. RHE. Dashed lines represent spectra calculated (adjusted) by a non-linear least squares program for the circuit $[R_s(Q_{dl}[R_{ad}W_{ad}C_{ad}])]$.

The inset to Fig. 3 illustrates the behavior of the capacitance spectra (40 mHz to 10 kHz, with decreasing frequencies clockwise) measured at 1.15 V in 0.5 M $H_2SO_4$ for pristine PtO film, and in pH-7.0 universal buffer for pristine PtO film and four PtO film electrodes modified by specific adsorption from four different aqueous solutions (see Section 2). A similar reasoning to that applied to Section 3.2 can explain the EIS results shown in the inset to Fig. 3 and in Table S5, which presents the values obtained for equivalent circuit ($[R_s(Q_{dl}[R_{ad}W_{ad}C_{ad}])]$) elements using a non-linear least squares program. The results shown in Table S5 do not differ from those previous discussed in Section 3.2, and using the $C_{ad}$ values to calculate $q$ from Eq. (2) and $Q$ from CV results, it was possible to calculate $N_{AS,PtO\ oxid}{}^{bloc}$ and $N_{AS,PtO\ red}{}^{bloc}$ (similarly to Eq. (4)).

The $N_{AS,PtO\ oxid}{}^{bloc}$ and $N_{AS,PtO\ red}{}^{bloc}$ results are shown in Table S6, revealing that CV experiments were more sensitive than EIS experiments. The number of active sites blocked by HM was calculated as $84 \times 10^{12}$ sites cm$^{-2}$ at the PtO/HM electrode and $25 \times 10^{12}$ sites cm$^{-2}$ at the PtO/M1 electrode, whereas the number of those blocked by MAP at the PtO/MAP electrode was $50 \times 10^{12}$ sites cm$^{-2}$. For the Pt/M2-Pt/M5 electrodes we assumed co-adsorption of HM (with MAP). The highest number of active sites blocked by MAP was found at the Pt/M4 electrode ($59 \times 10^{12}$ sites cm$^{-2}$ = (84–25) $\times 10^{12}$ sites cm$^{-2}$).

## 4. Conclusions

We demonstrated the feasibility of determining the number of active sites blocked by HM adsorbed alone or co-adsorbed with MAP. When the concentration of MAP in a specific adsorption solution is increased, the compound is more effectively co-adsorbed than HM (used at constant concentration). In this higher-concentration environment, however, the amount of co-adsorbed MAP is virtually the same as when used alone at a lower concentration for specific adsorption (assuming the amount of co-adsorbed HM does not vary in either case, not even in the presence of high concentrations of MAP in mixed solutions for specific adsorption). In the case of sequential specific adsorption, the first compound typically predominates over the second. In addition, EIS was more effective for determining the number of blocked active sites on Pt than CV, which was superior for PtO films.

Our approach can be applied to different studies involving noxious organic compounds (such as pesticides) or metals capable of adsorbing onto metal or metal oxide surfaces (and also onto environment systems such as soil minerals). The procedure therefore represents an alternative to batch experiments and other analytical techniques for quantification of these compounds.

## Acknowledgments

The authors wish to thank PROPP-UFMS, FUNDECT-MS (grants 23/200.044/2007 and 23/200.119/2007), CAPES, and CNPq (grants 620181/2006-0, 307408/2008-6 and 6200227/2008-8) for their financial support.

## Appendix A. Supplementary data

Supplementary data associated with this article can be found, in the online version, at doi:10.1016/j.jhazmat.2010.11.059.

## References

[1] N. Koleli, C. Kantar, U. Cuvalci, H. Yilmaz, Movement and adsorption of methamidophos in clay loam and sandy loam soils, Int. J. Environ. Anal. Chem. 86 (2006) 1127–1134.
[2] N. Koleli, A. Demir, H. Arslan, C. Kantar, Sorption behavior of methamidophos in a heterogeneous alluvial soil profile, Colloid Surf. A: Physicochem. Eng. Asp. 301 (2007) 94–99.
[3] K.D. Jones, W.-H. Huang, Evaluation of toxicity of the pesticides, chlorpyrifos and arsenic, in the presence of compost humic substances in aqueous systems, J. Hazard. Mater. B 103 (2003) 93–105.
[4] K. Dai, T. Peng, H. Chen, R. Zhang, Y. Zhang, Photocatalytic degradation and mineralization of commercial methamidophos in aqueous titania suspension, Environ. Sci. Technol. 42 (2008) 1505–1510.
[5] Q. Li, X. Wang, D. Yuan, Solid-phase extraction of polar organophosphorous pesticide from aqueous samples with oxidized carbon nanotubes, J. Environ. Monit. 11 (2009) 439–444.
[6] S.T. Han, J. Li, H.L. Xi, D.N. Xu, Y. Zuo, J.H. Zhang, Photocatalytic decomposition of acephate in irradiated $TiO_2$ suspensions, J. Hazard. Mater. 163 (2009) 1165–1172.
[7] B.S. Ismail, A.O.S. Enoma, U.B. Cheah, K.Y. Lum, Z. Malik, Adsorption, desorption, and mobility of two insecticides in Malaysian agricultural soi, J. Environ. Sci. Health B 37 (2002) 355–364.
[8] C. De Pasquale, A. Jones, A. Charlton, G. Alonzo, Use of SPME extraction to determine organophosphorus pesticides adsorption phenomena in water and soil matrices, Int. J. Environ. Anal. Chem. 85 (2005) 1101–1115.
[9] Y. Yu, Q.-X. Zhou, Adsorption characteristics of pesticides methamidophos and glyphosate by two soils, Chemosphere 58 (2005) 811–816.
[10] J.-H. Yen, K.-H. Lin, Y.-S. Wang, Potential of the insecticides acephate and methamidophos to contaminate groundwater, Ecotoxicol. Environ. Saf. 45 (2000) 79–86.
[11] A.P. Silva, S.S. Marqueti, G. Maia, Specific adsorption of propiconazole and humic acid on Pt and PtO films, Electrochim. Acta 54 (2009) 6896–6907.
[12] H.A. Menezes, G. Maia, Specific adsorption of arsenic and humic acid on Pt and PtO films, Electrochim. Acta 55 (2010) 4942–4951.
[13] H. Angerstein-Kozlowska, Surfaces, cells, and solutions for kinetics studies, in: E. Yeager, J.O'M. Bockris, B.E. Conway, S. Sarangapani (Eds.), Comprehensive Treatise of Electrochemistry, vol. 9, Plenum Press, New York, 1984, p. 24.
[14] W.R. Carmody, Easily prepared wide range buffer series, J. Chem. Educ. 38 (1961) 559–560.
[15] A.K. Singh, T. White, D. Spassova, Y. Jiang, Physicochemical, molecular-orbital and electronic properties of acephate and methamidophos, Comp. Biochem. Physiol. 119C (1998) 107–117.
[16] R.P. Schwarzenbach, P.M. Gschwend, D.M. Imboden, Environmental Organic Chemistry, second ed., John Wiley & Sons, Inc., New Jersey, 2003 (Chapter 11).
[17] C.A. Martínez-Huitle, A. De Battisti, S. Ferro, S. Reyna, M. Cerro-López, M.A. Quiro, Removal of the pesticide methamidophos from aqueous solutions by electrooxidation using $Pb/PbO_2$, $Ti/SnO_2$, and Si/BDD electrodes, Environ. Sci. Technol. 42 (2008) 6929–6935.
[18] T. Pajkossy, D.M. Kolb, Double layer capacitance of Pt(1 1 1) single crystal electrodes, Electrochim. Acta 46 (2001) 3063–3071.
[19] Z. Kerner, T. Pajkossy, Measurement of adsorption rates of anions on Au(1 1 1) electrodes by impedance spectroscopy, Electrochim. Acta 47 (2002) 2055–2063.
[20] T. Pajkossy, D.M. Kolb, Anion-adsorption-related frequency-dependent double layer capacitance of the platinum-group metals in the double layer region, Electrochim. Acta 53 (2008) 7403–7409.
[21] Z. Kerner, T. Pajkossy, L.A. Kibler, D.M. Kolb, The double layer capacity of Pt(1 0 0) in aqueous perchlorate solutions, Electrochem. Commun. 4 (2002) 787–789.
[22] O.I. González-Peña, Y.M. Vong, T.W. Chapman, R. Antaño-López, Study of adsorption of citrate on Pt by CV and EQCM, Electrochim. Acta 53 (2008) 5549–5554.